Ferrite Assisted Synchronous Reluctance Machines: a General Approach

(Article begins on next page)

02 September 2025

Ferrite Assisted Synchronous Reluctance Machines: a General Approach

A. Vagati, *Fellow, IEEE*, B. Boazzo, P. Guglielmi, *Member, IEEE*, G. Pellegrino, *Member, IEEE*

Abstract – **A general approach to the design of high performance ferrite-assisted synchronous reluctance motors is presented. Reference is made to a rectified rotor structure, with multiple flux barriers, designed to optimize the performance and the exploitation of the PM material. The key design issue of de-magnetization is analytically investigated, pointing out the maximum allowed current loading, depending on temperature and machine dimensions. Such current limit is then compared with the one imposed by the thermal constraint. The analysis shows that low and medium size machines tend to be robust against demagnetization, while larger machines are more at risk. The theoretical analysis is confirmed by finite-elements via an example machine design.**

Index Terms—**Ferrite, IPM Synchronous motors, Synchronous Reluctance, Demagnetization, Large pole number.**

I. INTRODUCTION

The adoption of Permanent Magnet (PM) machines in controlled drives is continuously increasing, because of the well-known qualities of large torque density, high efficiency, precise speed control, etc. Both Surface Mounted PM (SPM) and Interior PM (IPM) types of rotors are used, with some differences in performance, depending on the application [1, 2]. The most used PM materials are based on rare-earths, in the most of cases NdFeB is preferred, because of the large remanence values.

However, the rare-earths availability has recently become quite critical, because of the high cost volatility due to the monopolistic policy of the main producing country. This is way electric drive designers are compelled to find some alternative solution, especially in those applications where the PM quantity is significant (e.g. large wind turbine generators) or has a significant impact on cost, like in mass production (e.g. drives for automotive, home appliances, etc.).

The mere substitution of Nd-based magnet with a low cost one (e.g. ferrite) would lead to a lower performance, in general. In fact, an SPM rotor would evidently have a much lower airgap flux density and consequently a poor torque density.

Flux concentration IPM rotor structures can improve the airgap flux density, but still not reaching torque density values comparable with those of Nd based SPM machines.

A viable alternative to PM based torque production is to adopt reluctance based one so to use the PMs only for adjusting the power factor of high saliency synchronous reluctance machines. PM-assisted synchronous reluctance motors have a torque density that is comparable with the one of SPM machines while needing a limited PM quantity (in case it is Nd), or, otherwise, their flux barriers can be filled

Alfredo Vagati, Barbara Boazzo, Gianmario Pellegrino and Paolo Guglielmi are with Politecnico di Torino, Department of Energy, Corso Duca degli Abruzzi 24, 10129 Torino, Italy. The e-mails are: (alfredo.vagati, barbara.boazzo, gianmario.pellegrino, paolo.guglielmi @polito.it)

with greater quantities of the less performing ferrite magnets, still obtaining similar performance [7-9].

The paper deals with Ferrite-Assisted Synchronous Reluctance (FASR) machines with a multiple barrier rotor structure, having large saliency ratios and then a considerable saliency torque. All flux barriers (layers) are completely filled with ferrite magnets, to get the most in terms of PM flux linkage out of the low energy density material.

Ferrite PMs, indeed, are more prone to demagnetization than rare earth magnets. This requires the current loading to be limited accordingly, with the consequences of a potential limitation of the obtainable torque density. Such limitation has no counterpart in Nd-based IPM motors. As a consequence, the machine design must specifically deal with this point, at the aim of maximizing the obtainable performance.

In this paper, a general approach to this problem is presented, particularly devoted to high pole number machines. It will be shown that the demagnetizing constraint does not represent an effective limitation for small and medium size machines, while it becomes more compelling for large machines, e.g. for large direct drive wind turbines generators.
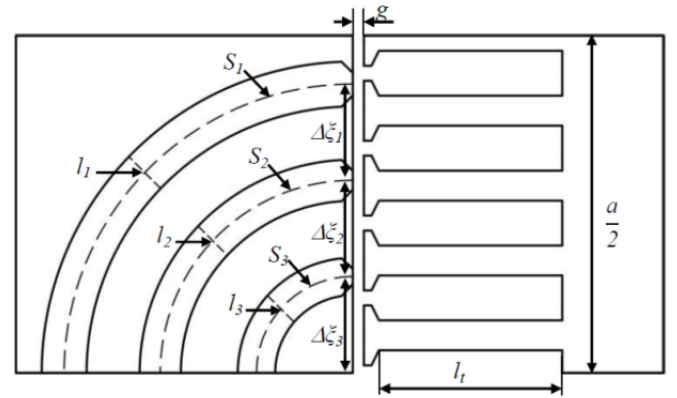

Fig. 1.   Reference geometry: rectified machine, half pole, three layers rotor ($n = 3$, $n_r = 14$)

II. GENERAL APPROACH AND EQUIVALENT CIRCUIT

Before starting any analytical investigation, a simplified (but realistic) reference geometry has to be defined.

The proposed per-unit model is based on an elementary block, representing one pole of a FASR machine by the schematic rectified structure shown in Fig. 1. The reference block geometry is very near to the effective shape of the machine poles when high pole numbers (e.g. 16 poles or more) are considered, as it is the case of low speed wind generators and torque motors. Dealing with lower pole number, such as for medium to high speed applications, the rectified structure represents a worst case analysis. Thus, the chosen linear-machine-like template is a good starting point for a comprehensive analysis.

In general, with PM-Assisted Synchronous Reluctance

(PMASR) motors, the design starts with the maximization of the rotor anisotropy and hence the reluctance torque. As it is known [3, 4], the rotor saliency decreases as the pole number is increased, because of the reduced airgap permeance and also because the barrier widths (S_k) increase with respect to the pole pitch. From this point of view, a machine with two poles would be the best choice, but it has no room for shaft embedding and thus is heavily limited by iron saturation. From four poles on, given the airgap length and the pole arc, the machine saliency depends mainly on the layer number n and on the average permeance of the flux barriers, which have to be properly designed for optimizing the saliency ratio and minimizing the interferences between stator and rotor space harmonic fields.

A. Reference geometry

The elementary block shown in Fig. 1 is an example of a three layer structure, schematically represented with round shaped barriers for the sake of simplicity.

The key-geometric parameters introduced in Fig.1 are:

- the airgap length g;
- the pole pitch a;
- the tooth length l_t;
- the airgap rotor pitch $\Delta\xi_k$;
- half the width S_k of the kth layer and its length l_k.

When the flux barriers have to be filled with ferrite, having all the PM material equally exploited is the most reasonable choice to cope with the demagnetization problem and layers with constant length (l_k) are preferred. In fact, thickening the flux barriers around their axis of symmetry (i.e. in their central part) slightly increases the saliency ratio, but the thinner sections of a layer would suffer from de-magnetization more than the thicker ones.

Dealing with the torque ripple minimization, the flux barriers displacement along the rotor periphery has to be properly chosen [4,5]. The inter-barrier pitch is usually kept constant and equal to $\Delta\xi_r$ (1), following definite rules to match the stator slots number with the quantity n_r, which represents the number of equivalent rotor slots per pole pair.

$$\Delta\xi_r = \frac{2\pi}{n_r} \tag{1}$$

Conversely, the angle $\Delta\xi_n$ ($\Delta\xi_3$ in Fig. 1) between the smaller layer and the q-axis (i.e. the minimum inductance direction) can be made also larger than the regular pitch. When $\Delta\xi_n > \Delta\xi_r$, the rotor structure is called incomplete, while, if $\Delta\xi_n = \Delta\xi_r$, the rotor is called complete [5]. In this second case, once the flux barriers number n is fixed, the constant pitch $\Delta\xi_r$ together with the parameter n_r are implicitly defined and vice versa.

In the following, reference will be made to complete structures, to limit the degrees of freedom and simplify the form of equations. Anyway the results can be easily extended to incomplete machines.

B. Per-unit equivalent circuit

The equivalent magnetic circuit of the 3-layer example geometry is reported in Fig. 2, allowing calculation of the rotor magnetic performance when all the stator m.m.f is applied against the magnets (defined as the "quadrature" direction in a PMASR machine). This situation represents the worst case, concerning demagnetization.

Analogously, the structural ribs connecting the rotor flux guides are not included in the magnetic model, though they are an important design variable, normally involved in the rotor equivalent circuit [2,5]. In fact, the rib presence tends to preserve the magnets from demagnetization, as it will be shown with the FEA example in the last Section. This is why it is safe here to adopt the simplified circuital model with no rib terms.
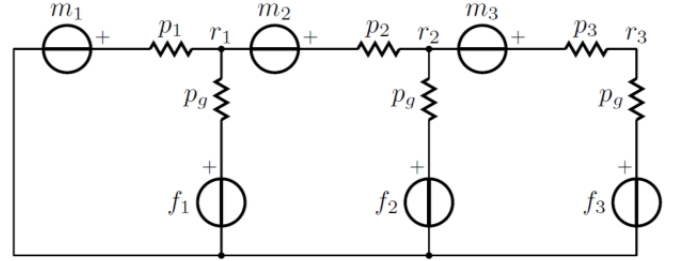

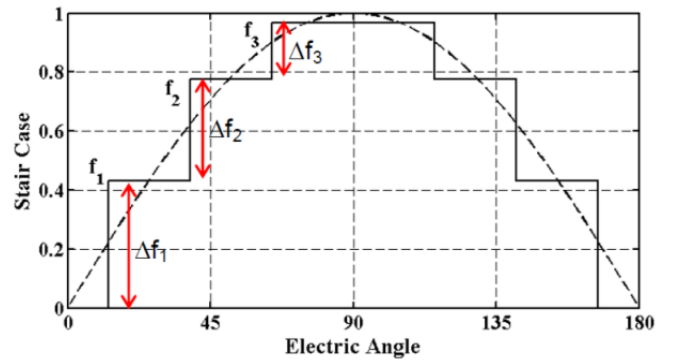Fig. 2. Equivalent circuit of the three layer rotor machine

Fig. 3. Unitary staircase m.m.f. distribution (f_k and Δf_k)

Reference is made in the equivalent circuit to p.u. quantities, both for m.m.f generators and permeance values. The former are referred to the peak F_q of the stator q-axis m.m.f, while the latter are divided by $\mu_0 l$, being l the active stack length. Consequently the fluxes are normalized with respect to $\mu_0 F_q l$. Of course, effective values can be obtained simply by multiplying each parameter by the corresponding reference quantity.

$$m_k = \frac{\frac{B_r}{\mu_0} l_k}{F_q} \tag{2}$$

(B_r is the magnet remanence).

The circuit proposed in Fig. 2 is based on the assumption that the magnetic potential along each rotor flux guide is constant and equal to the p.u. values r_k. The p.u. magnet m.m.f.s are represented by the m_k (2) generators, while the f_k ones model the m.m.f. applied by the stator. If a sinusoidal m.m.f. shape is supposed, the f_k have the staircase values obtained by averaging the sinusoid over each rotor pitch ($\Delta\xi_r$). This is shown by Fig. 3, still with reference to $n=3$, where a unitary m.m.f. distribution is represented, since F_q has been chosen as reference quantity.

In Fig. 2, the magnetic permeance of the flux barriers p_k (3) and that of the adjacent segment at the airgap p_g (4) have been evidenced as well. In Eq. (3), S_k and l_k are "equivalent" width and length, respectively, because of the layer tapering close to the airgap, while Eq. (4) puts in evidence that the

same airgap permeance is valid for all the circuit branches when complete structures are considered, since $\Delta\xi_k = \Delta\xi_r = const$.

$$p_k = \frac{S_k}{l_k} \quad (3)$$

$$p_g = \frac{a\Delta\xi_r}{\pi k_c g} \quad (4)$$

(k_c is the Carter coefficient)

C.   Analytical model

A generic solution of the circuit described in Fig. 2 can be obtained with Eq. (5), whose vectors are shown by (6) in the case $n=3$.

$$A \cdot \Delta r = B \cdot m + C \cdot \Delta f \quad (5)$$

$$\Delta r = \begin{bmatrix} \Delta r_1 \\ \Delta r_2 \\ \Delta r_3 \end{bmatrix} = \begin{bmatrix} r_1 \\ r_2 - r_1 \\ r_3 - r_2 \end{bmatrix}$$

$$m = \begin{bmatrix} m_1 \\ m_2 \\ m_3 \end{bmatrix} \quad (6)$$

$$\Delta f = \begin{bmatrix} \Delta f_1 \\ \Delta f_2 \\ \Delta f_3 \end{bmatrix} = \begin{bmatrix} f_1 \\ f_2 - f_1 \\ f_3 - f_2 \end{bmatrix}$$

Matrixes *A,B* and *C* in Eq.(5) have generally a complex form, but they become really simple if the m.m.f.s m_k and the flux barrier permeances p_k are designed to make *Δr* proportional to *Δf*. The purpose of this design choice is two-fold:

- it minimizes the harmonic content of the quadrature flux density [5];
- all the magnets work at the same flux density.

In particular, for making *Δr* proportional to *Δf* in all load conditions (including the no load working point), the p.u. vector *m* has to be proportional to *Δf* as in (7), where the peak value *M* of the magnet m.m.f. is referred to the main harmonic.

$$m = \frac{M}{F_q}\Delta f \quad (7)$$

Remembering (2) and pointing out that the ratio M/F_q will be sufficiently larger than one to protect the magnets from demagnetization, Eq. (7) implies to design the magnet according to (8),

$$l_k = \Delta f_k \frac{\sum_n l_k}{\sum_n \Delta f_k} = \Delta f_k \frac{l_a}{f_a} \quad (8)$$

where the total insulation length l_a is introduced.

In addition to (7), in order to minimize the quadrature flux density harmonic content by making *Δr* proportional to *Δf*, when complete rotor structures are considered, constant barrier permeance design ($p_k = p_b = const$) has to be adopted.

According to this design approach, the matrixes in Eq. (5) can be easily written as in Eq. (9). Reference is still made to *n=3*, but they can be easily extended to the general case.

$$A = \begin{bmatrix} \beta+1 & -\beta & 0 \\ 1 & \beta+1 & -\beta \\ 1 & 1 & \beta+1 \end{bmatrix} \quad where\ \beta = \frac{p_b}{p_g}$$

$$B = \begin{bmatrix} \beta & -\beta & 0 \\ 0 & \beta & -\beta \\ 0 & 0 & \beta \end{bmatrix} \quad C = \begin{bmatrix} 1 & 0 & 0 \\ 1 & 1 & 0 \\ 1 & 1 & 1 \end{bmatrix} \quad (9)$$

Besides, if Eq. (7) is valid and $p_k = p_b = const$, it follows from (5) that also the p.u. flux values $(m_k - r_k)\ p_b$ are proportional to Δf_k, confirming that the working flux density of the magnets becomes the same for all layers. In fact, the effective magnet flux density B_m referred to the magnet remanence B_r depends on the ratio $\Delta r_k\ /m_k$, as defined in (10).

$$(B_{m,pu})_k = \frac{B_m}{B_r} = 1 - \frac{\Delta r_k}{m_k} = B_{m,pu} \quad (10)$$

III.   DEMAGNETIZATION ANALYSIS

A.   No load working point

From (5), by dropping out the *Δf* vector, the no load *Δr* is obtained. Substituting the so calculated *Δr* into (10), Eq. (11) is found. Eq. (11) gives the magnets working point, which is the same for all the *n* barriers according to the previous assumptions.

$$B_{m0,pu} = \frac{1}{1 + \frac{S_1}{l_a}\frac{g}{a}\frac{2\pi}{\Delta\xi_r}\sin\left(\frac{\Delta\xi_r}{2}\right)} \quad (11)$$

Since one half the rotor pitch is a relatively small angle for large n_r numbers, the term $sin(\Delta\xi_r/2)/\Delta\xi_r$ tends to *1/2*. Thus, the number of rotor barriers is lightly affecting the $B_{m0,pu}$ calculation, which mainly depends on the ratios: S_1/l_a and *a/g*. The former term (S_1/l_a) is constrained by the geometry, while the latter (*a/g*) must be sufficiently large, to avoid excessive small no-load flux density values in the magnets. In fact, reduced values in PM flux density would lead to demagnetization, especially at very low temperature, as it is clear from the example ferrite characteristics given in Fig. 7.

If the additional approximation is made that S_1 has a circular shape (Fig. 1), then (12) is valid. By substituting into (11), Eq. (14) is found where the p.u. magnetic insulation $l_{a,pu}$ (13) has been introduced.

Let us observe that in the approximated form, the rotor pitch disappears. Anyway, the results coming from the complete (11) are reported in Fig. 4, where the negligible effect of the number of layers *n* (and then of n_r) is evidenced. On the other hand the influence of *a/g* on the no-load working point is significant and large *a/g* are strongly suggested, at least beyond *80* or more. The p.u. insulation $l_{a,pu}$ looks also important, although it is less affecting the result, as the ratio *a/g* is increased.

$$S_1 = \left(\frac{n_r - 2}{4}\right)\Delta\xi_r\frac{a}{2} = \frac{\pi}{4}a\left(1 - \frac{2}{n_r}\right) \quad (12)$$

$$l_{a,pu} = \frac{l_a}{a/2} \quad (13)$$

$$B_{m0,pu} = \cfrac{1}{1 + \cfrac{\pi^2}{l_{a,pu}} \cfrac{\sin\left(\cfrac{\Delta\xi_r}{2}\right)}{\Delta\xi_r} \cfrac{g}{a}\left(1 - \cfrac{2}{n_r}\right)} \cong \qquad (14)$$

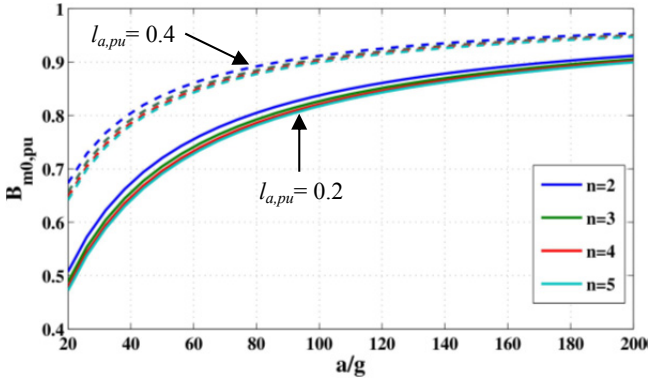$$\cong \cfrac{1}{1 + \cfrac{\pi^2}{2l_{a,pu}} \cfrac{g}{a}}$$

Fig. 4   No load p.u. flux density in the magnets for different number of layers and total insulation lengths : dashed lines $l_{a,pu}$ = 0.4, continuous lines $l_{a,pu}$ = 0.2

B.   Working point at load

From (5) and (10) the p.u. magnets flux density corresponding to an applied peak m.m.f. F_q can be calculated. In practice, the opposite is wanted.

Once the magnetic material is chosen and the design temperature is fixed, the minimum p.u. flux density value $B_{md,pu}$ not to have demagnetization is known. The maximum m.m.f. $F_{q,max}$ can be then calculated by Eq. (15), where f_a is defined in (8). The m.m.f. per pole ($F_{q,max}/a$ ratio) in (15) is equivalent to the linear current density or specific current loading.

$$\frac{F_{q,max}}{a} = \frac{B_r}{2\mu_0 f_a} l_{a,pu} \left(1 - \frac{B_{md,pu}}{B_{m0,pu}}\right) \qquad (15)$$

Let us point out that B_r depends on the temperature and increases as the temperature is decreased, but also the flux density corresponding to the de-magnetization point increases as the temperature is decreased. As a consequence, at cold, large $B_{md,pu}$ limit values have to be considered, to prevent demagnetization (Fig. 7), but the larger B_r values counteract and limit the net temperature effect on the available specific current loading given by (15). On the other hand, at hot temperature, the B_r value is quite lower and the allowed $B_{md,pu}$ value is low too or even becomes negative, thus leading to a situation which is effectively better for the demagnetization risk (Fig. 7).

With reference to the example case $n=3$, in Fig. 5 plots are given of the maximum m.m.f. per pole coming from the demagnetization limit.

The $F_{q,max}/a$ ratio is represented as a function of a/g and depends both on the working temperature and the p.u. insulation length $l_{a,pu}$. Differently from Fig. 4, the influence of this two parameter is here quite relevant, but, as for $B_{m0,pu}$, $F_{q,max}/a$ is asymptotic with a/g, confirming that a/g values lower than 80 strongly limit the design with respect to the demagnetization problem.

If in the plots of Fig. 5 sufficiently large a/g values are

considered, at cold (-50°C, $B_{md,pu}$=0.55), the maximum m.m.f. per pole overcomes 20000Aturn/m only when $l_{a,pu}$ is close to 0.4, while at 130°C ($B_{md,pu}$=-0.1) with the same p.u. insulation length the allowed m.m.f. nearly doubles.

This suggests first that *the machine current loading limit is not so critical, when very low working temperatures can be excluded.*

On the other hand, when critical design temperatures have to be taken into account, there is a limit to the current loading (depending on the temperature) that cannot be overcome, since the dependence on a/g is asymptotic and $l_{a,pu}$ is strongly limited by the geometry, especially if the hypothesis of constant barrier length, $l_{a,pu}$ is made. In fact, since sufficient room for the iron flux guides has to be preserved, $l_{a,pu}$ could hardly reach 0.4 for complete machines, while its value decreases (e.g. to 0.3) when the rotor structure is incomplete. This leads to set an upper limit to the m.m.f. per pole of a complete machine around 25000A$_{turn}$/m, at -50°C, no matter how much the machine designer is skilled, at least with the magnetic material shown in Fig. 7.

As conclusive remarks to this demagnetization analysis, let us remember that a/g represents nothing else than the pole permeance at the airgap, while the p.u. insulation $l_{a,pu}$ is indicative someway of the q-axis reluctance. As a consequence, *a design which is safe for demagnetization is also an high anisotropy design.*
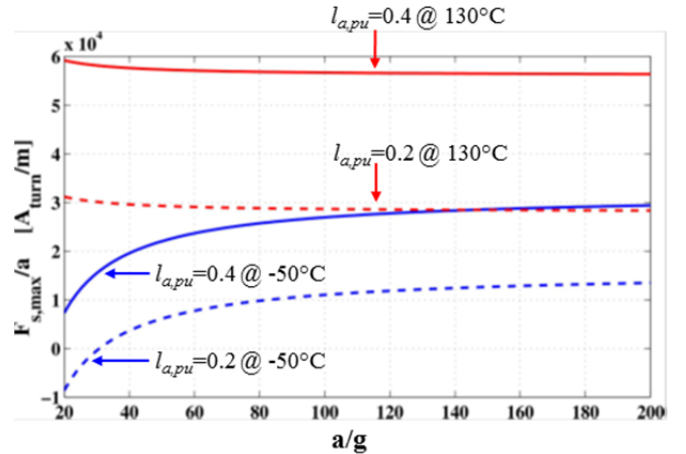

Fig. 5   Allowable m.m.f. per pole: dashed line $l_{a,pu}$ =0.2, continuous line $l_{a,pu}$ =0.4. Red lines refer to 130°C while blue lines refer to -50°C.

IV.   EFFECT OF THE MACHINE SIZE

The current loading limit coming from the demagnetization risk is nearly independent on the machine size. On the contrary, the thermal limit generally is, as known. The larger the machine size D is, the lower the current density is, which has to decrease as $D^{-0.5}$ if the same power dissipation per outer machine surface (k_j) is wanted. However, since the copper section increases as D^2, the m.m.f. per pole will increase as $D^{0.5}$. This is shown by Eq. (16), which is easily derived by assuming a sinusoidal m.m.f. shape at the aigap. Equal slot and tooth widths are also supposed, for simplicity.

$$\frac{F_{q,th}}{a} = \frac{k_w}{\pi} \sqrt{\frac{k_j k_{cu}}{k_{end}\rho_{cu}}} \sqrt{l_t} \qquad (16)$$

The shown coefficients are:
- k_{cu} the fill in factor
- k_j the specific dissipation (at the outer surface)
- k_w the usual winding coefficient
- k_{end} average half turn length divided by l;
- ρ_{cu} the copper resistivity.
- l_t the tooth length.

When the cross sectional shape is defined, l_t just stands for the machine dimension D.

To get an idea of the effect of (16), Fig. 6 is shown, with reference to $k_j = 10000$W/m^2 and $k_j = 3500$W/m^2, and to the following values: $k_{cu} = 0.4$, $k_{end} = 1.5$, $\rho_{cu} = 25 \cdot 10^{-9}\Omega$/m (at 130°C) and $k_w = 0.92$. The hot copper resistivity is considered, since the rated current value is referred to. From (16), the tooth length giving 25000A$_{turn}$/m (cold ferrite limit) becomes 0,07 m. Let us observe that this value strongly depends on k_j. A value of 10000W/m^2 requires water cooling, while a natural cooling value (e.g. 3500W/m^2) would have led to a crossover tooth length of 0.2 m.

Anyway, for a defined cooling system, Fig. 6 splits the machines into low sized (left) and large sized (right). Low sized machines can be overloaded with respect to their continuous duty till demagnetization limit. The opposite is true for large machines, for which the ferrite demagnetization limit overcomes the thermal constraint: no overload current is allowed, in this case. Of course, when the very low temperatures can be excluded, the impact of the ferrite demagnetization becomes lower and the crossover l_t values move to larger sized machines.
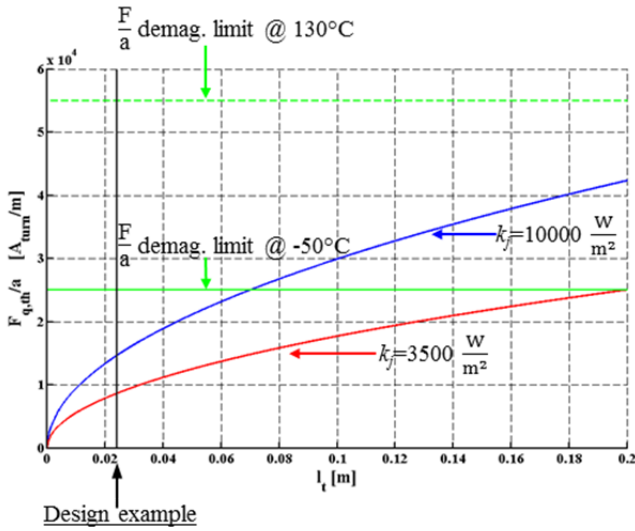

Fig. 6   Per pole m.m.f. versus tooth length: k_j =10000W/m^2 (blue line), k_j=3500W/m^2(red line). Demagnetization level @-50°C (green line), @130°C (green line dotted).

V.   DESIGN EXAMPLE

To give a concrete idea of the obtained performance, a design example is presented. The reference motor ratings are given in Table I, while stator and rotor shapes are reported in Figs. 8, 10 and 11, together with some field plots.

The machine has twelve poles and the rotor is complete (constant rotor pitch). The stator has three slots per pole phase and three winding layers (shifted by one slot, to properly reduce torque ripple).

As said, the design procedure started with the maximization of the reluctance torque and hence the rotor anisotropy. In this case the saliency ratio reaches about 13, if cross saturation and rib effect are disregarded as well as the stator leakage inductances. Due to the rib presence and the cross saturation effect, the saliency ratio decreases to 8 and it drops near to 5 considering all the stator leakage components (slot, zig-zag, end winding). In general, the reduction of the saliency ratio due to the stator leakage is far from negligible. That is why the machine split ratio (rotor diameter/outer stator diameter) is usually increased as the pole number is increased, to reduce the tooth length l_t and limit at least the slot leakage component.

In the example case, which has a quite large number of poles, l_t is 24mm. Then, the m.m.f. per pole coming from the thermal constraint (16) is 17300 A$_{turn}$/m. It's lower than the ferrite limit (15), which would be 25000 A$_{turn}$/m with $a/g = 95$ and $l_{a,pu} = 0.375$. It follows that this machine can be considered as *small sized*, that is having transient overload capability.
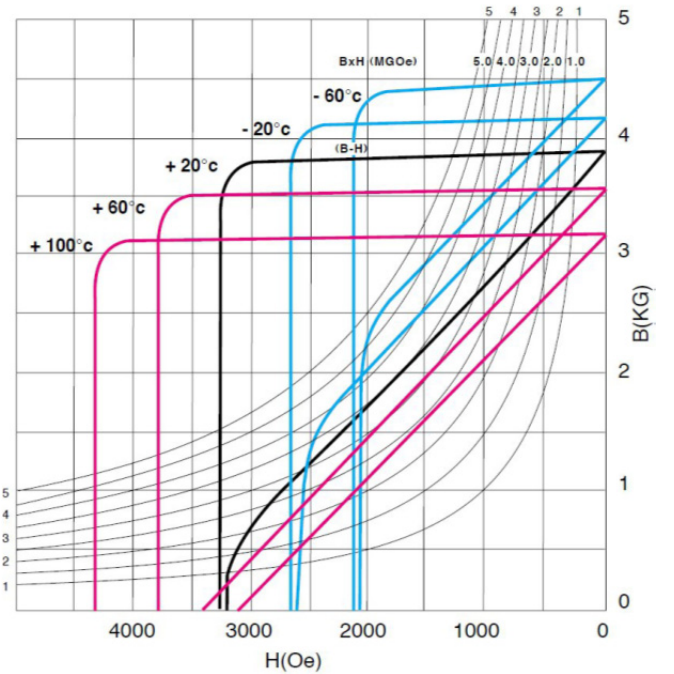

Fig. 7   BH characteristics of the considered ferrite grade (USF by CALAMITE)

TABLE I – DETAILS OF THE EXAMPLE MOTOR

Active length	260	mm
External diameter	380	mm
Poles	12	-
Pole to airgap ratio (a/g)	95	-
Tooth length (l_t)	24	mm
Number of flux barriers	3	-
Nominal Speed	200	rpm
Rated Torque	800	Nm
Specific losses k_j	10000	W/m^2
Thermal limit (16)	17300	A$_{turn}$/m
Demag. limit @ -50 (15)	25000	A$_{turn}$/m

The ferrite quantity embedded into the rotor is sufficient to compensate the q-axis flux completely, as shown by the

vector diagram of Fig. 9, where the q-axis resulting flux is slightly negative. This result is obtained at hot temperature (130°C), that is when the PM action is more limited (the remanence drops down to 0.32T, in this case). The power factor obtained at 130 °C is quite good, up to 0.95 due to a torque angle near to 70°. This angle will further increase, of course, at colder temperatures. In fact, the motor performance remains very good, in spite of the quite large PM flux variation (Fig. 9). This is another relevant advantage of the PM Assisted SyR motor, which has a low sensitivity to PM remanence variations.
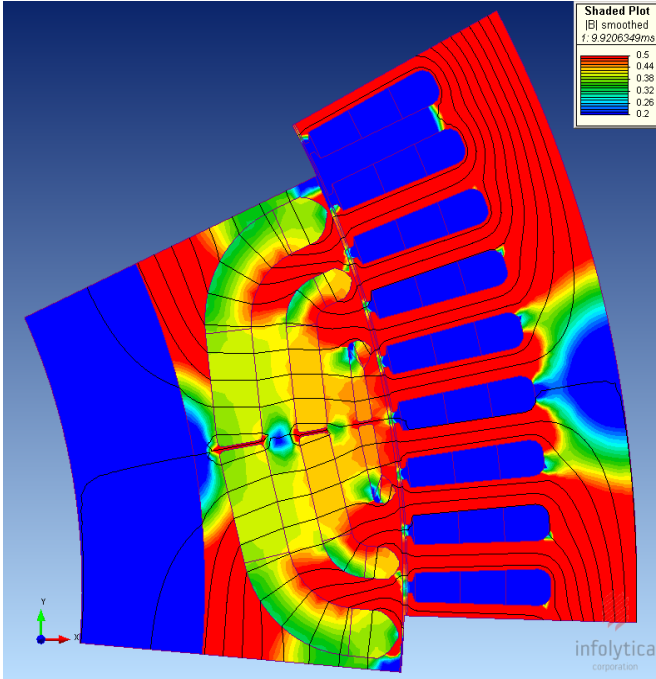

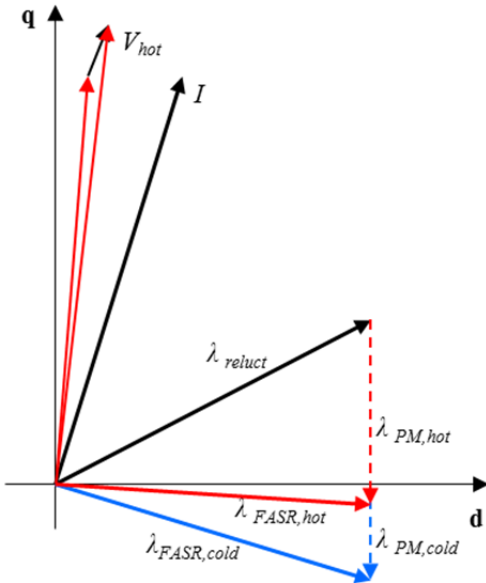
Fig. 8   FEA: @-50°C no-load

Fig. 9   Vector diagram for the example motor, at continuous current (thermal limit). "Hot" refers to PMs at 130°C, while "cold" refers to -50°C.

Let us now consider the results of some FE simulations. In Fig 8 a no load situation is reported, at – 50 °C, while Fig. 11 shows the rated load situation, at the same temperature.

In general, it is pointed out that the curved shape of the flux barriers enhance demagnetization in the inner border of the barrier. This is an expected situation, that could not be considered in the approximated formulas presented in Section III, of course. In spite of that, the ferrite situation at rated current is safe from demagnetization, due to the current loading quite lower than the limit in Fig. 6 (17300 A_{turn}/m vs 25000 A_{turn}/m). Instead, in Fig. 10 a current loading is referred to just beyond the limit (nearly 25000 A_{turn}/m), still at -50°C. The ferrite situation in the borders of the barriers looks now definitely critical, as expected. This is a further verification of the validity of the previously made analysis.

No FE simulations at hot temperature are reported, since the analysis of Section III has clearly excluded any risk, as shown by Fig. 6.
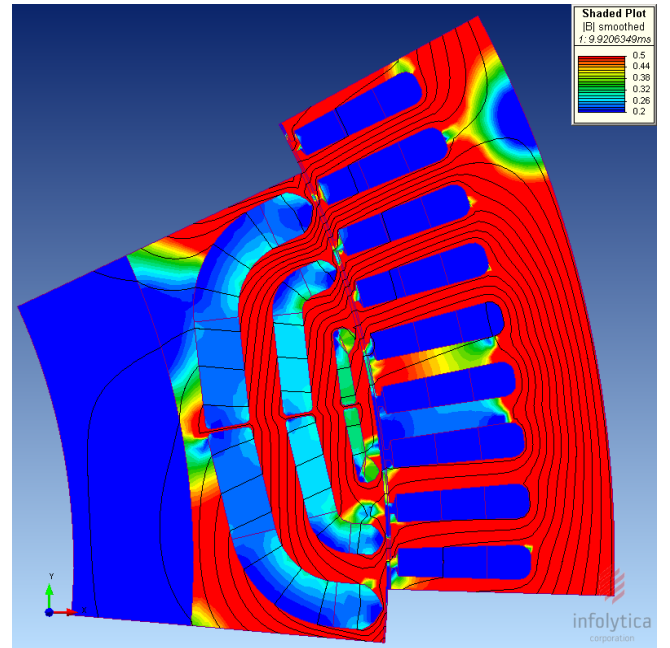

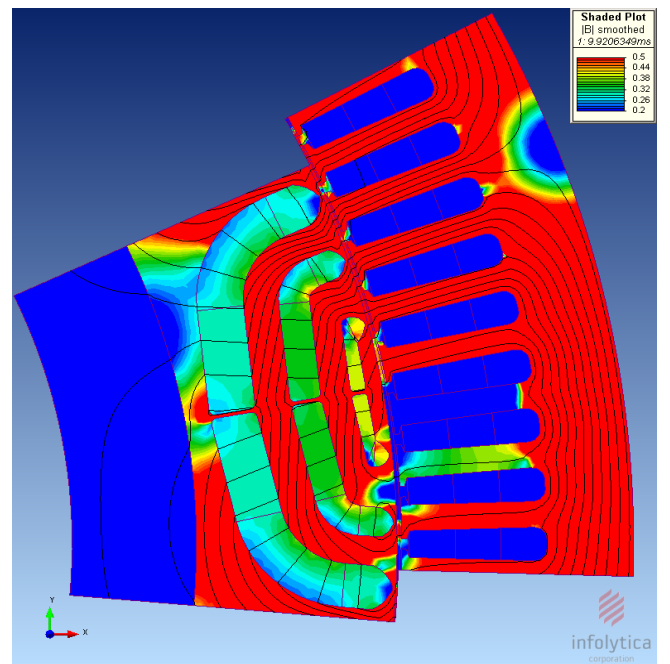Fig. 10   FEA: @-50°C, maximum current loading according to demagnetization limit (15)

Fig. 11   FEA @-50°C, current loading according to thermal limit (16)

VI. CONCLUSIONS

The paper shows that synchronous reluctance machines assisted by low cost ferrite magnets can effectively compete with the most expensive rare earth based PM machines. The most effective rotor design is based on constant-length flux barriers, resulting in uniform exploitation of the PM material. The allowed current loading has been calculated analytically and validated by FEA with good accordance. The dependence of the machine performance on machine size and working temperature has been pointed out. Except for very large machines and very low temperature values, the current demagnetization limit is far from being critical. As a consequence, the proposed FASR machine is well suited for both high and low speed applications, markedly where cost saving and/or good flux weakening performance are of main interest.

VII. REFERENCES

[1] Pellegrino, G.; Vagati, A.; Guglielmi, P.; Boazzo, B.; , "Performance Comparison Between Surface-Mounted and Interior PM Motor Drives for Electric Vehicle Application," *Industrial Electronics, IEEE Transactions on* , vol.59, no.2, pp.803-811, Feb. 2012.

[2] El-Refaie, A.M.; Jahns, T.M., "Comparison of synchronous PM machine types for wide constant-power speed range operation," Industry Applications Conference, 2005. Fourtieth IAS Annual Meeting. Conference Record of the 2005 , vol.2, no., pp. 1015- 1022 Vol. 2.

[3] A. Vagati and P. Guglielmi, "Design, analysis and control of Interior PM synchronous machines". ISBN 88-7178-898-2, sponsored by IEEE-Electrical Machine Committee, edited by CLEUP, Padova, Italy, 2004, ch. Design of PM assisted synchronous reluctance (PMASR) motors, pp. 6.1-6.35.

[4] R.R. Moghaddam, "Synchronous Reluctance Machine (SynRM) in Variable Speed Drives (VSD) Applications". ISBN 978-91-7415-972-1, PhD Doctoral Thesis, edited by KTH, Stockholm, SWEDEN, 2011.

[5] A. Vagati, M. Pastorelli, G. Franceschini, and S. Petrache, "Design of low-torque-ripple synchronous reluctance motors," Industry Applications, IEEE Transactions on, vol. 34, no. 4, pp. 758 -765, jul/aug 1998.

[6] E. Armando, P. Guglielmi, G. Pellegrino, and A. Vagati, "Optimal design of IPM-PMASR motors for wide constant power speed range," in Power Conversion & Intelligent Motion Conference, 22-24 May 2007, Nurnberg, Germany.

[7] Chino, S.; Ogasawara, S.; Miura, T.; Chiba, A.; Takemoto, M.; Hoshi, N.; "Fundamental characteristics of a ferrite permanent magnet axial gap motor with segmented rotor structure for the hybrid electric vehicle," Energy Conversion Congress and Exposition (ECCE), 2011 IEEE , vol., no., pp.2805-2811.

[8] Sanada, M.; Inoue, Y.; Morimoto, S.; "Rotor structure for reducing demagnetization of magnet in a PMASynRM with ferrite permanent magnet and its characteristics," Energy Conversion Congress and Exposition (ECCE), 2011 IEEE , vol., no., pp.4189-4194.

[9] Armando, E.; Guglielmi, P.; Pastorelli, M.; Pellegrino, G.; Vagati, A.; "Performance of IPM-PMASR Motors with Ferrite Injection for Home Appliance Washing Machine," Industry Applications Society Annual Meeting, 2008. IAS '08. IEEE , vol., no., pp.1-6.

Alfredo Vagati (M'88–SM'92–F'98) received the Laurea degree in Electrical Engineering from Politecnico di Torino, Turin, Italy, in 1970.

After a few years working in industry with Olivetti, he joined Politecnico di Torino in 1975, as Assistant Professor. In 1990, he became Professor of Electrical Machines and Drives at the University of Cagliari, Italy. In 1991, he rejoined Politecnico di Torino in the same capacity. From 1995 to 2003 He was the Head of the Electrical Engineering Department of Politecnico di Torino and member of the Academic Senate from 2005 to 2009. His scientific activity, in the field of electrical machines and drives, has been focused on high-performance ac drives. He has been involved in several industrial projects in the field of ac drives, as both a designer and a scientific reference. His most relevant activity has concerned the design and control of a family of newly developed, high-performance synchronous reluctance (SyR) an permanent magnet assisted synchronous reluctance (PMASR) motors. He has led several national and European research projects in the field of design and control of synchronous-machine-based drives for many different applications, including home appliances and the automotive world. He has authored or coauthored more than 100 technical papers.

Prof. Vagati is a Fellow Member of the IEEE Society. He is also a member of the Advisory Board of PCIM, International Conference and Exhibition.

Barbara Boazzo received the M.Sc. degree in electrical engineering from Politecnico di Torino in 2010. She is currently a PhD student at the same university, working in the field of electric motors and drives.

Paolo Guglielmi (M'07) received the M.Sc. degree in electronic engineering and the Ph.D. degree in electrical engineering from the Politecnico di Torino, Turin, Italy, in 1996 and 2001, respectively.

In 2002, he joined the Department of Electrical Engineering, Politecnico di Torino, as Assistant Professor and becomes an Associate Professor in 2012.

He has authored several papers published in technical journals and conference proceedings. His fields of interest include power electronics, high performance drives, and computer-aided design of electrical machines.

Gianmario Pellegrino (M'06) received the M.Sc. and Ph.D. degrees in electrical engineering from Politecnico di Torino, Turin, Italy, in 1998 and 2002, respectively. He has been a Guest Researcher at Aalborg University, Denmark, in 2002. Since 2002 he has been with Politecnico di Torino, first as a Research Associate and then as an Assistant Professor, since 2007. He has been a visiting fellow at Nottingham University, UK, in 2010/2011. He is involved in research projects within the industry. He has more than 50 technical papers and one patent. His research areas are the electrical machines and drives, namely, the motor design and the digital control. Dr. Pellegrino is an Associate Editor for the IEEE Transactions on Industry Applications. He is the corecipient of the IEEE-IAS EMC 3rd Paper Paper Award for ECCE 2009, the IEEE-IAS IDC 3rd Paper Paper Award for ECCE 2010 and the ICEM 2010 Best Paper Award.